EURASIP Journal on Advances in Signal Processing
a SpringerOpen Journal

RESEARCH Open Access

Motion parameter estimation of multiple ground moving targets in multi-static passive radar systems

Saurav Subedi[1], Yimin D Zhang[1*], Moeness G Amin[1] and Braham Himed[2]

Abstract

Multi-static passive radar (MPR) systems typically use narrowband signals and operate under weak signal conditions, making them difficult to reliably estimate motion parameters of ground moving targets. On the other hand, the availability of multiple spatially separated illuminators of opportunity provides a means to achieve multi-static diversity and overall signal enhancement. In this paper, we consider the problem of estimating motion parameters, including velocity and acceleration, of multiple closely located ground moving targets in a typical MPR platform with focus on weak signal conditions, where traditional time-frequency analysis-based methods become unreliable or infeasible. The underlying problem is reformulated as a sparse signal reconstruction problem in a discretized parameter search space. While the different bistatic links have distinct Doppler signatures, they share the same set of motion parameters of the ground moving targets. Therefore, such motion parameters act as a common sparse support to enable the exploitation of group sparsity-based methods for robust motion parameter estimation. This provides a means of combining signal energy from all available illuminators of opportunity and, thereby, obtaining a reliable estimation even when each individual signal is weak. Because the maximum likelihood (ML) estimation of motion parameters involves a multi-dimensional search and its performance is sensitive to target position errors, we also propose a technique that decouples the target motion parameters, yielding a two-step process that sequentially estimates the acceleration and velocity vectors with a reduced dimensionality of the parameter search space. We compare the performance of the sequential method against the ML estimation with the consideration of imperfect knowledge of the initial target positions. The Cramér-Rao bound (CRB) of the underlying parameter estimation problem is derived for a general multiple-target scenario in an MPR system. Simulation results are provided to compare the performance of the sparse signal reconstruction-based methods against the traditional time-frequency-based methods as well as the CRB.

Keywords: Multi-static passive radar; Sparse reconstruction; Group sparsity; Motion parameter estimation

1 Introduction

Multi-static passive radar (MPR) has recently attracted significant research interests primarily due to its low cost and covertness compared to a conventional radar system. Also, since passive radar systems use signals of opportunity as transmitters, they do not exacerbate the problem of spectral congestion [1]. MPR systems are typically characterized by low signal power, narrow signal bandwidth, bistatic mode of operation, and availability of multiple spatially separated transmitters, rendering them significantly different from conventional radar systems. From a signal processing perspective, operation in low signal-to-noise ratio (SNR) conditions exploiting narrowband signals creates additional challenges for target detection, localization, and tracking. On the other hand, availability of several spatially separated illuminators can be exploited to achieve a higher effective SNR and multi-static diversity [2].

Motion parameter estimation of ground moving targets has been studied extensively in the context of

*Correspondence: yimin.zhang@villanova.edu
[1]Center for Advanced Communications, Villanova University, Villanova, PA 19085, USA
Full list of author information is available at the end of the article

conventional radar systems (e.g., single-antenna radar [3], phased-array radar [4], and multiple-input multiple-output (MIMO) radar [5-7]). Several advanced signal processing techniques, including time-frequency analysis, motion compensation, and range migration compensation (e.g., [8-10]), have been developed for the detection and parameter estimation of moving targets based on their Doppler signatures. However, limited work has been done in estimating target motion parameters in MPR systems (e.g., [11,12]). In this paper, we investigate the problem of motion parameter estimation of ground moving targets in a multi-static passive airborne radar.

Existing motion parameter estimation techniques (e.g., [13-15]) are based on time-frequency analysis of Doppler signatures of received signals, which are commonly modeled as general-order polynomials [16]. For a moderately long coherent processing interval (CPI), it suffices to model the target motion by a second-order polynomial or a linear frequency-modulated signal. As such, time-frequency analysis methods are used to estimate the chirp parameters followed by a mapping to the actual target motion parameters. When multiple targets are present, the Doppler signature of the radar return is modeled as a linear sum of multiple chirp signals [17].

In low SNR situations, as encountered in typical MPR systems, reliable estimation of chirp parameters for each bistatic link may become difficult. As such, it is desirable to enhance the overall signal quality either by extending the CPI or by exploiting the availability of multiple bistatic links. The state of the art for estimating motion parameters of closely spaced multiple ground moving targets in typical MPR systems is incomplete, because of the rather non-trivial two issues:

1. Since the Doppler signature corresponding to each bistatic link cannot be reliably estimated, and it is rather difficult to directly combine them in the time-frequency domain for overall signal enhancement, traditional methods based on time-frequency analysis cannot effectively benefit from the availability of multiple transmitters.
2. Although a longer CPI can be used to enhance the SNR corresponding to each bistatic link, the target range migration must be compensated for before processing the signal over the azimuthal time. A longer CPI, however, requires the consideration of higher-order motion parameters (e.g., acceleration and jerk) which are more difficult to estimate and compensate. This further limits the applicability of time-frequency analysis-based methods, particulary for highly accelerating (or decelerating) targets.

A motion parameter estimation method based on sparse signal reconstruction has recently been developed [2], which coherently combines data from all available illuminators of opportunity and, thereby, achieves overall signal enhancement and multi-static diversity. This method involves a sequential estimation process, where the target acceleration is estimated by coherently fusing all the signal observations mapped into the ambiguity function of the respective Doppler signature and detecting the combined peak via a direct search. The estimated value of target acceleration is then used in the estimation of the target velocity by exploiting sparse signal reconstruction. However, the applicability of this method is limited to a single-target scenario. Multiple closely spaced targets may be frequently encountered in MPR systems due to the small signal bandwidth and the corresponding poor range resolution. A method based on exhaustive search becomes computationally inefficient for such a multiple-target scenario because its computational complexity increases exponentially with the number of targets.

In this paper, with the *a priori* knowledge that Doppler signatures corresponding to multiple illuminators of opportunity share the same set of motion parameters, i.e., velocity and acceleration of targets, as a common sparse support, we develop a new motion parameter estimation technique exploiting the group sparsity-based signal reconstruction. This enables us to effectively fuse data corresponding to all available illuminators to accumulate sufficient signal energy without further extending the CPI. Also, contributions from more illuminators, if available, can be utilized for a better performance. In order to reduce the computational load associated with the motion parameter estimation of multiple closely located targets, we also propose a sequential process which estimates target acceleration and velocity vectors in tandem. We consider the effect of an imperfect knowledge of target positions, which causes phase differences among Doppler signatures corresponding to different bistatic links. As a result, the performance of methods based on coherent fusion of these Doppler signatures may significantly degrade depending on the phase interactions. On the contrary, the sequential method based on group sparsity is robust to such phase interactions, as it only assumes that a common sparsity support is shared among all available bistatic links. The Cramér-Rao bound (CRB) for the underlying parameter estimation problem is derived for a general target distribution scenario in an MPR system, and simulation results are provided to compare the performance of the proposed methods against the theoretical bound. The performance of the sparse signal reconstruction-based methods is also compared against traditional methods based on time-frequency analysis for motion parame-

ter estimation of two closely located ground moving targets.

The rest of the paper is organized as follows. Section 2 formulates the signal model for the Doppler signature in a multi-target scenario considering a multi-static passive radar network configuration. Section 3 presents the motion parameter estimation algorithms, including a brief review of the time-frequency analysis-based method and the description of the proposed techniques that are based on maximum likelihood (ML) and sequential estimations, both exploiting the group sparsity of target motion parameters. The effect of imperfect knowledge of the initial target positions on the motion parameter estimation is also examined in Section 3. Section 4 derives the CRB for the underlying parameter estimation problem. Section 5 presents simulation results that compare the estimation accuracy of the ML and sequential estimation methods against the CRB as well as the traditional time-frequency analysis-based methods. Finally, conclusions are drawn in Section 6.

The following notations are used in this paper. A lower (upper) case bold letter denotes a vector (matrix). In particular, $\mathbf{I}_N$ denotes the $N \times N$ identity matrix. $(.)^*$, $(.)^T$, and $(.)^H$, respectively, denote complex conjugation, transpose, and Hermitian operations. $\|\cdot\|_1$ and $\|\cdot\|$, respectively, denote the l_1 and l_2 norm of a vector, whereas $\Re(.)$ and $\Im(.)$, respectively, stand for the real part of a complex number, and $\mathcal{CN}(a,b)$ denotes standard complex normal distribution with mean a and variance b. In addition, diag(.) and tr(.), respectively, denote the diagonal and trace operations.

2 Signal model

2.1 Geographical relationship

We consider a problem of estimating motion parameters of multiple, closely located, ground moving targets in a typical MPR system. We assume that the MPR system operates in a multiple-frequency network, i.e., N broadcast stations, located at $\mathbf{b}^{(n)}$, $n = 1,\ldots,N$, transmit waveforms in non-overlapping frequency bands which are respectively centered at $f^{(n)}$, $n = 1,\ldots,N$. These stations are assumed stationary and their locations precisely known *a priori*.

An airborne receiver, initially located at $\mathbf{r}_0$, is assumed to be moving along its track direction with a uniform velocity $\mathbf{v}_r$, whereas there are K closely located ground moving targets. The kth target is assumed to be initially located at $\mathbf{p}_0^{(k)}$, moving with an initial velocity of $\mathbf{v}^{(k)}$ and an acceleration of $\mathbf{a}^{(k)}$. Because only ground targets are considered, the z-axis components of $\mathbf{p}_0^{(k)}$, $\mathbf{v}^{(k)}$, and $\mathbf{a}^{(k)}$ are assumed to be zero.

The direct range between the nth illuminator and the receiver, corresponding to the reference channel, is defined as

$$r^{(n)}(t) = \|\mathbf{r}(t) - \mathbf{b}^{(n)}\|, \tag{1}$$

where $\mathbf{r}(t) = \mathbf{r}_0 + \mathbf{v}_r t$ represents the trajectory of the receiver at time t. Likewise, the bistatic range between the nth transmitter, the kth target, and the receiver is expressed as

$$\rho^{(n,k)}(t) = \|\mathbf{p}^{(k)}(t) - \mathbf{b}^{(n)}\| + \|\mathbf{p}^{(k)}(t) - \mathbf{r}(t)\|, \tag{2}$$

where $\mathbf{p}^{(k)}(t) = \mathbf{p}_0^{(k)} + \mathbf{v}^{(k)}t + \frac{1}{2}\mathbf{a}^{(k)}t^2$ represents the trajectory of the kth target at time t.

2.2 Reference and surveillance signals

The direct path signal received from the nth transmitter can be expressed as

$$s_{\mathrm{r}}^{(n)}(t) = u^{(n)}\left(t - r^{(n)}(t)/c\right)\exp\left(-j2\pi f^{(n)} r^{(n)}(t)/c\right) + \eta_{\mathrm{r}}^{(n)}(t), \tag{3}$$

where the subscript 'r' represents the reference channel, $u^{(n)}(t)$ is the baseband representation of the signal transmitted from the nth illuminator, c is the velocity of wave propagation, and $\eta_r(t)$ represents the additive noise. Since passive radars use broadcast signals, it can be assumed that the transmitted signal is perfectly reconstructed at the receiver after demodulation and forward error correction [18]. Therefore, the direct path signal, after reconstruction and error correction, becomes

$$s_{\mathrm{r}}^{(n)}(t) = u^{(n)}(t - r^{(n)}(t)/c)\exp\left(-j2\pi f^{(n)} r^{(n)}(t)/c\right), \tag{4}$$

which is used as the reference signal.

The surveillance signal reflected from the kth target corresponding to the signal transmitted by the nth illuminator is

$$\begin{aligned} s_{\mathrm{s}}^{(n,k)}(t) = {} & \sigma^{(n,k)} u^{(n)}\left(t - \rho^{(n,k)}(t)/c\right) \\ & \times \exp\left(-j2\pi f^{(n)}\rho^{(n,k)}(t)/c\right) + \eta_{\mathrm{s}}^{(n)}(t), \end{aligned} \tag{5}$$

where the subscript 's' denotes the surveillance channel, $\sigma^{(n,k)}$ is the target reflection coefficient corresponding to the kth target, and $\eta_{\mathrm{s}}^{(n)}(t)$ is the additive noise.

2.3 Matched filtering and range migration correction

At the receiver, the surveillance signal is correlated with the reference signal, yielding a sequence of the matched

filter output. The phase term of the output of the matched filter is determined by the difference between the bistatic transmitter-target-receiver range and the direct transmitter-receiver range. Denote Δt as the azimuthal sampling interval used in the matched filtering, and $t_m = m\Delta t$ be the azimuthal sampling instants, $m = 0, \ldots, M-1$. Then, the range difference at the mth azimuthal sampling instant, t_m, can be expressed as

$$\begin{aligned} R^{(n,k)}(t_m) &= \rho^{(n,k)}(t_m) - r^{(n)}(t_m) \\ &= \left\| \mathbf{p}_0^{(k)} + \mathbf{v}^{(k)} t_m + \mathbf{a}^{(k)} t_m^2/2 - \mathbf{b}^{(n)} \right\| \\ &\quad + \left\| \mathbf{p}_0^{(k)} + \mathbf{v}^{(k)} t_m + \mathbf{a}^{(k)} t_m^2/2 - \mathbf{r}_0 - \mathbf{v}_r t_m \right\| \\ &\quad - \left\| \mathbf{r}_0 + \mathbf{v}_r t_m - \mathbf{b}^{(n)} \right\|. \end{aligned} \tag{6}$$

From (6), it can be inferred that motion of ground moving targets and motion of the radar platform are the two sources of range migration. In view of a typical MPR system, due to the narrow signal bandwidth and, consequently, the low bistatic range resolution, target range migration is not a critical issue for a short or moderate CPI. However, when an extended CPI is required, e.g., in very weak signal conditions, target range migration must be properly compensated for. The commonly used range migration compensation methods, such as the Keystone transform [19], can be used to compensate for the linear range migration. However, when acceleration and higher order motion parameters are prominent features of the target motion, target range migration compensation emerges as a challenging problem. In the underlying problem, we consider a moderately long CPI, which obviates the need for target range migration compensation.

On the other hand, since motion parameters of the receiver platform are precisely known, we can compensate for the range migration due to its movement [15] about a ground reference position in close vicinity of the actual position of targets, referred to as scene origins. For the kth target, considering a scene origin at $\mathbf{q}^{(k)}$, the bistatic range between the nth transmitter, the scene origin, and the receiver can be calculated at the mth azimuthal sampling instant as

$$\zeta^{(n)}(t_m) = \|\mathbf{q}^{(k)} - \mathbf{b}^{(n)}\| + \|\mathbf{q}^{(k)} - \mathbf{r}(t_m)\|. \tag{7}$$

Therefore, after compensating for the range migration due to the movement of the receiver platform, the range difference at azimuthal time t_m can be expressed as

$$\begin{aligned} \tilde{R}^{(n,k)}(t_m) &= \rho^{(n,k)}(t_m) - \zeta^{(n,k)}(t_m) \\ &= \left\| \mathbf{p}^{(k)}(t_m) - \mathbf{b}^{(n)} \right\| + \left\| \mathbf{p}^{(k)}(t_m) - \mathbf{r}(t_m) \right\| \\ &\quad - \left\| \mathbf{q}^{(k)} - \mathbf{b}^{(n)} \right\| - \left\| \mathbf{q}^{(k)} - \mathbf{r}(t_m) \right\| \\ &= \left\| \mathbf{p}_0^{(k)} + \mathbf{v}^{(k)} t_m + \mathbf{a}^{(k)} t_m^2/2 - \mathbf{b}^{(n)} \right\| \\ &\quad + \left\| \mathbf{p}_0^{(k)} + \mathbf{v}^{(k)} t_m + \mathbf{a}^{(k)} t_m^2/2 - \mathbf{r}_0 - \mathbf{v}_r t_m \right\| \\ &\quad - \left\| \mathbf{q}^{(k)} - \mathbf{b}^{(n)} \right\| - \left\| \mathbf{q}^{(k)} - \mathbf{r}_0 - \mathbf{v}_r t_m \right\|. \end{aligned} \tag{8}$$

2.4 Observed Doppler signature

The signal transmitted by each of the N illuminators is reflected by the K moving targets, and hence, the signal arriving at the receiver is the superposition of radar returns from the K targets. Thus, the output of the receiver matched filter at azimuthal time t_m corresponding to the nth illuminator, after range migration compensation due to the motion of the receiver platform at the scene origin, can be expressed as a linear sum of K different Doppler signatures,

$$s^{(n)}(t_m) = \sum_{k=1}^{K} \xi^{(n,k)} \exp\left(j2\pi f^{(n)} \tilde{R}^{(n,k)}(t_m)/c \right) + \eta^{(n)}(t_m), \tag{9}$$

where $\xi^{(n,k)} = \xi_R^{(n,k)} + j\xi_I^{(n,k)}$ is a complex number representing the magnitude of the matched filter output corresponding to the return from the kth target, and $\eta^{(n)}(t_m)$ is the additive Gaussian white noise output. The complex magnitude $\xi^{(n,k)}$ can be assumed time-invariant because the target radar cross-section (RCS) for a given bistatic pair does not fluctuate significantly over the given observation period. Note that the unknown initial phase component due to the complex target reflectivity $\sigma^{(n,k)}$ is absorbed in the unknown complex magnitude $\xi^{(n,k)}$. The phase term of the matched filter output, as discussed in the preceding section, is determined by the range difference, depicted in (8).

Considering a moderately long CPI, the Doppler signature from each target can be modeled as a second-order phase polynomial signal, or referred to as a linear chirp. That is, the phase term of $s^{(n,k)}(t_m)$, denoted as $\phi^{(n,k)}(t_m)$, follows a quadratic relationship:

$$\phi^{(n,k)}(t_m) = \phi_0^{(n,k)} + 2\pi f_0^{(n,k)} t_m + \pi \beta^{(n,k)} t_m^2, \tag{10}$$

where $\phi_0^{(n,k)}$ is the initial phase, $f_0^{(n,k)}$ is the initial Doppler frequency, and $\beta^{(n,k)}$ is the chirp rate.

3 Motion parameter estimation

In this section, we analyze the motion parameter estimation of multiple ground moving targets in the given multi-static passive network configuration using the time-frequency analysis and group sparsity-based signal reconstruction method.

3.1 Motion parameter estimation using time-frequency analysis

As described in Section 2, the Doppler signature corresponding to a ground moving target can be modeled as a linear chirp for a moderate CPI. The chirp parameters, i.e., the initial frequency and chirp rate, can be estimated using time-frequency analysis techniques such as the Radon-Wigner transform, the fractional Fourier transform (FrFT), and the chirp-Fourier transform. These methods have been widely used in various radar applications (e.g., [20-24]). A motion parameter estimation method, for single as well as multiple closely located ground moving targets, is proposed in [15]. The method proposed in [15] assumes *a priori* knowledge of Doppler signature parameters corresponding to all bistatic links, obtained using the time-frequency analysis, to estimate motion parameters using

$$\begin{bmatrix} f_0^{(n,k)} \\ \beta^{(n,k)} \end{bmatrix} = \mathbf{A}^{(n,k)} \left(\mathbf{q}^{(\mathbf{k})} \right) \begin{bmatrix} \mathbf{v}^{(k)} \\ \mathbf{a}^{(k)} \end{bmatrix}, \tag{11}$$

where $f_0^{(n,k)}$ and $\beta^{(n,k)}$, respectively, are the initial Doppler frequency and the chirp rate observed in the signature corresponding to the nth transmitter and target motion parameters $\mathbf{v}^{(k)}$ and $\mathbf{a}^{(k)}$ of the kth target. The matrix $\mathbf{A}^{(n,k)}(\mathbf{q}^{(\mathbf{k})})$, which maps the chirp parameters to the respective motion parameter, is defined as

$$\mathbf{A}^{(n,k)} \left(\mathbf{q}^{(\mathbf{k})} \right) = \frac{1}{\lambda^{(n)}} \begin{bmatrix} \frac{\left(\mathbf{q}^{(k)} - \mathbf{b}^{(n)} \right)^T}{\| \mathbf{q}^{(k)} - \mathbf{b}^{(n)} \|} + \frac{\left(\mathbf{q}^{(k)} - \mathbf{r}_0 \right)^T}{\| \mathbf{q}^{(k)} - \mathbf{r}_0 \|} & \mathbf{0} \\ -\frac{2\mathbf{v}_r^T}{\| \mathbf{q}^{(k)} - \mathbf{r}_0 \|} & \frac{\left(\mathbf{q}^{(k)} - \mathbf{b}^{(n)} \right)^T}{\| \mathbf{q}^{(k)} - \mathbf{b}^{(n)} \|} + \frac{\left(\mathbf{q}^{(k)} - \mathbf{r}_0 \right)^T}{\| \mathbf{q}^{(k)} - \mathbf{r}_0 \|} \end{bmatrix}, \tag{12}$$

where $\lambda^{(n)}$ is the wavelength of the signal corresponding to the the nth transmitter. For N spatially separated transmitters, we obtain $2N$ distinct equations. Therefore, the four unknown motion parameters of each target can be unambiguously estimated when $N \geq 2$.

However, under weak signal conditions, it is difficult to obtain reliable chirp parameter estimations using time-frequency analysis of the Doppler signatures. In the presence of additive white Gaussian noise, the chirp parameter estimation process exhibits a threshold effect in the sense that, when SNR is below a certain threshold, there is a rapid performance degradation [24]. As discussed earlier, despite the availability of several transmitters, the Doppler signatures corresponding to different bistatic links are distinct in general and thus cannot be directly combined in the time-frequency domain to improve the estimation reliability and accuracy of the chirp parameters in each bistatic pair.

In the following, we consider exploiting the group sparsity-based signal reconstruction for motion parameter estimation. This helps achieve overall signal enhancement by combining information from all possible bistatic links and, thereby, obtaining a reliable motion parameter estimation even in weak signal conditions.

3.2 Motion parameter estimation using sparse signal reconstruction

In (8), we see that the motion of a target is determined by four unknown motion parameters, i.e., the x- and y-axis components of its acceleration and velocity. With the *a priori* information that Doppler signatures corresponding to different bistatic links share the same set of motion parameters, the problem can be modeled as a group sparse signal reconstruction problem.

In the underlying problem, the measurement matrix needs to represent a discretized four-dimensional (4-D) space of the unknown motion parameters, such that each point in the discretized space represents a hypothetical combination of target motion parameters (v_x, v_y, a_x, a_y). It is noted that the true motion parameters can assume any value in the continuous space and an attempt to represent the motion parameters in a discretized 4-D space may result in an 'off-grid' problem. However, by adequately sampling the parameter space, a good performance can be achieved as long as the mutual coherence among the columns of the measurement matrix is low enough to permit the sparse signal reconstruction. The performance of the sparsity-based signal reconstruction method can be improved by increasing the resolution of the measurement matrix. However, this increases a risk of increasing the mutual coherence among the columns of the dictionary matrix to an extent where sparse reconstruction becomes impractical or infeasible. Considering these two issues, it is important to define the measurement matrix as fine as possible provided that the sparse reconstruction is feasible. Mathematically, it is possible to obtain a joint estimation of multiple-target motion parameters through an ML search.

3.2.1 *Maximum likelihood estimation*

The $N \times 1$ received signal vector at the mth azimuthal sampling instant, t_m, can be formed as

$$\mathbf{s}(t_m) = \left[s^{(1)}(t_m), s^{(2)}(t_m), \cdots, s^{(N)}(t_m) \right]^T = \boldsymbol{\gamma}(t_m) + \boldsymbol{\eta}(t_m), \tag{13}$$

where $s^{(n)}(t_m)$ is the output of the receiver matched filter defined in (9),

$$\boldsymbol{\gamma}(t_m) = \sum_{k=1}^{K} \boldsymbol{\Theta}^{(k)}(t_m)\boldsymbol{\xi}^{(k)}, \tag{14}$$

where $\boldsymbol{\Theta}^{(k)}(t_m) = \text{diag}\left\{\left[\exp\left(j2\pi f^{(1)}\tilde{R}^{(1,k)}(t_m)/c\right), \cdots, \exp\left(j2\pi f^{(N)}\tilde{R}^{(N,k)}(t_m)/c\right)\right]^T\right\}$, $\boldsymbol{\xi}^{(\mathbf{k})} = \left[\xi^{(1,k)}, \cdots, \xi^{(N,k)}\right]^T$, and $\boldsymbol{\eta}(t_m)$ represents the $N \times 1$ additive Gaussian noise vector. As such, the received signal vector can be modeled as a complex multivariate normally distributed random variable, such that

$$\mathbf{s}(t_m) \sim \mathcal{CN}\left(\boldsymbol{\gamma}(t_m), \sigma^2\mathbf{I}_N\right). \tag{15}$$

In the underlying problem, the unknown parameter set can be defined as $\boldsymbol{\vartheta} = (\boldsymbol{\xi}, \mathbf{a}, \mathbf{v})$, where $\boldsymbol{\xi} = \left[(\boldsymbol{\xi}^{(1)})^T, \cdots, (\boldsymbol{\xi}^{(K)})^T\right]^T$, $\mathbf{a} = \left[(\mathbf{a}^{(1)})^T, \cdots, (\mathbf{a}^{(K)})^T\right]^T$, and $\mathbf{v} = \left[(\mathbf{v}^{(1)})^T, \cdots, (\mathbf{v}^{(K)})^T\right]^T$. The respective unknown vectors corresponding to the kth target are defined as $\boldsymbol{\xi}^{(\mathbf{k})} = \left[\xi^{(1,k)}, \cdots, \xi^{(N,k)}\right]^T$, $\mathbf{a}^{(k)} = \left[a_x^{(k)}, a_y^{(k)}\right]^T$, and $\mathbf{v}^{(k)} = \left[v_x^{(k)}, v_y^{(k)}\right]^T$.

Then, the negative log-likelihood function of the unknown parameters is given as

$$\mathcal{L}(\boldsymbol{\vartheta}) = \sum_{m=0}^{M-1} \|\mathbf{s}(t_m) - \boldsymbol{\gamma}(t_m)\|^2. \tag{16}$$

The target parameters can be estimated by minimizing (16) over the unknown parameters. Therefore, the ML estimator can be defined as

$$\hat{\boldsymbol{\vartheta}} = \arg\min_{\boldsymbol{\vartheta}} \mathcal{L}(\boldsymbol{\vartheta}). \tag{17}$$

However, from a practical standpoint, the ML estimation based on (17) requires a computationally demanding 4-D parameter search.

In the following, we propose a two-step sequential estimation process to reduce the dimensionality of the parameter search space. First, we obtain estimates of target acceleration by applying group sparsity-based signal recovery in the ambiguity domain. Then, the estimated values of target acceleration are used for estimating velocities of the respective targets.

3.2.2 Estimation of acceleration of multiple targets

It is established in [2] that, for a radar return whose Doppler signature is characterized as a chirp, the chirp rate depends largely on the target acceleration, whereas the initial velocity of the target has an insignificant effect on the chirp rate, specially when the target-receiver distance is large. It can be inferred from (12) that, for a large target-receiver separation, the matrix $\mathbf{A}^{(n,k)}(\mathbf{q}^{(\mathbf{k})})$ becomes nearly block diagonal, almost decoupling the effect of velocity and acceleration of a target on its Doppler signature. It is also known that, when a chirp signal is considered in the ambiguity domain, its signature is not affected by its initial frequency. That is, the ambiguity function of a target's Doppler signature is a straight line passing through the origin, irrespective of the initial Doppler frequency, where the slope of the straight line is determined by the chirp rate. With multiple targets, the ambiguity function auto-terms of the radar return, defined in (9), constitutes multiple lines which all pass through the origin but with different slopes, depending on the respective target accelerations. By applying group sparsity-based signal reconstruction methods in the ambiguity domain, therefore, it is possible to simultaneously utilize the signal energy in all available bistatic links for estimating the acceleration of multiple targets, using the process detailed as follows.

The ambiguity function of the signal $s^{(n)}(t_m)$ corresponding to the Doppler frequency θ and time delay τ is defined in the discrete-time representation as

$$\chi^{(n)}(\theta,\tau) = \sum_{m=0}^{M-1} s^{(n)}(t_m+\tau)\left[s^{(n)}(t_m-\tau)\right]^* \exp(-j2\pi\theta t_m). \tag{18}$$

The discretized two-dimensional (2-D) ambiguity function corresponding to the nth broadcast station forms a matrix $\boldsymbol{\chi}^{(n)} \in \mathcal{C}^{N_\theta \times N_\tau}$, where N_θ and N_τ, respectively, represent the number of Doppler bins and the number of delay bins considered in the analysis.

In order to estimate the target acceleration by applying group sparsity-based signal reconstruction in the ambiguity domain, we define an $N_\theta N_\tau \times 1$ observation vector $\tilde{\mathbf{x}}^{(n)} = \text{vec}[\boldsymbol{\chi}^{(n)}]$ by vectorizing the discretized 2-D ambiguity function corresponding to the nth transmitter, where $n = 1, \cdots, N$. The entire acceleration space is represented by a 2-D discrete space comprising N_{ax} and N_{ay} points along the x-axis and y-axis, respectively. Let an $N_{ax}N_{ay} \times 1$ vector $\mathbf{u}^{(n)}$ be the unknown sparse vector which vectorizes the discretized 2-D acceleration space such that the pth element of $\mathbf{u}^{(n)}$ is associated with the pth hypothetical target acceleration vector $\mathbf{a}_{[p]} = [a_{x,n_{ax}}, a_{y,a_{ny}}, 0]^T$, where $a_{x,n_{ax}}$ and $a_{y,n_{ay}}$ are respectively the n_{ax}th discretized value in the N_{ax} x-direction acceleration points and the n_{ay}th discretized value in the N_{ay} y-direction acceleration points, and $p = (n_{ay}-1)N_{ax} + n_{ax} \in [1, N_{ax}N_{ay}]$. As such, the pth column of the dictionary matrix, $\boldsymbol{\Psi}^{(n)}$, that relates $\mathbf{u}^{(n)}$ and $\tilde{\mathbf{x}}^{(n)}$, is the vectorized 2-D ambiguity function when a hypothetic target acceleration is present at the pth entry of $\mathbf{u}^{(n)}$ with

a unit signal strength. To explicitly express the pth column of the dictionary matrix, we notice that, in this case, the bistatic range at the mth azimuthal sampling instant, after performing range migration compensation, can be obtained from (8) as

$$\begin{aligned}\tilde{R}_{[p]}^{(n,k)}(t_m) = &\left\|\mathbf{p}_0^{(k)} + \mathbf{a}_{[p]}t_m^2/2 - \mathbf{b}^{(n)}\right\| \\ &+ \left\|\mathbf{p}_0^{(k)} + \mathbf{a}_{[p]}t_m^2/2 - \mathbf{r}_0 - \mathbf{v}_r t_m\right\| \\ &- \|\mathbf{q}^{(k)} - \mathbf{b}^{(n)}\| - \left\|\mathbf{q}^{(k)} - \mathbf{r}_0 - \mathbf{v}_r t_m\right\|.\end{aligned} \tag{19}$$

Since the target velocity does not have a significant impact on the ambiguity function of the chirp Doppler signature, the velocity vector for all the targets is ignored in (19). As such, using (9), the output of the receiver matched filter at the mth azimuthal sample can be expressed as

$$s_{[p]}^{(n)}(t_m) = \sum_{k=1}^{K} \exp\left(j2\pi f^{(n)} \tilde{R}_{[p]}^{(n,k)}(t_m)/c\right). \tag{20}$$

The corresponding ambiguity function in the discrete-time representation is defined as

$$\chi_{[p]}^{(n)}(\theta,\tau) = \sum_{m=0}^{M-1} s_{[p]}^{(n)}(t_m+\tau)\left[s_{[p]}^{(n)}(t_m-\tau)\right]^* \exp(-j2\pi\theta t_m). \tag{21}$$

Vectorizing $\boldsymbol{\chi}_{[p]}^{(n)}$, whose (θ,τ)th element is $\chi_{[p]}^{(n)}(\theta,\tau)$, we obtain the pth column of the dictionary matrix $\boldsymbol{\Psi}^{(n)}$ as an $N_\theta N_\tau \times 1$ column vector defined as $\boldsymbol{\psi}_{[p]}^{(n)} = \mathrm{vec}\left[\boldsymbol{\chi}_{[p]}^{(n)}\right]$. Therefore, the unknown sparse vector representing the acceleration space, $\mathbf{u}^{(n)}$, can be obtained as the group sparse solution of the following linear formula:

$$\tilde{\mathbf{x}}^{(n)} = \boldsymbol{\Psi}^{(n)}\mathbf{u}^{(n)}, \quad n = 1,\ldots,N. \tag{22}$$

In this group sparse problem, the sparse vectors $\mathbf{u}^{(n)}$ share a common sparse support because the target accelerations are common to all N bistatic links, whereas the non-zero elements of $\mathbf{u}^{(n)}$, in general, differ for each n because of, among others, the imperfect estimation of initial target position and propagation attenuations. There are a number of algorithms available to solve the group sparse problems such as group basis pursuit [25], group LASSO [26], and block orthogonal matching pursuit [27]. Multi-task Bayesian compressive sensing algorithm [28,29] provides an adaptive learning framework and generally outperforms the conventional compressive sensing algorithms. In this paper, we use the complex multi-task Bayesian compressive sensing (CMT-BCS) algorithm [29], which is based on the Bayesian framework that exploits the statistical relationship between multiple measurements or sensing tasks and exploit the group sparsity between real and imaginary parts of the sparse entries. Also, since the CMT-BCS algorithm is known to be less sensitive to the dictionary coherence, it is a good choice for the underlying problem where it is desirable to have a high resolution measurement matrix. Since we deal with the complex data, we adopt a commonly used technique [29,30] to decompose the complex observation into its real and imaginary parts, and rewrite the nth observation vector as

$$\tilde{\mathbf{y}}^{(n)} = \left[\Re(\tilde{\mathbf{x}}^{(n)})^T, \Im(\tilde{\mathbf{x}}^{(n)})^T\right]^T \tag{23}$$

and the corresponding dictionary matrix as

$$\tilde{\boldsymbol{\Psi}}^{(n)} = \begin{bmatrix} \Re(\boldsymbol{\Psi}^{(n)}) & -\Im(\boldsymbol{\Psi}^{(n)}) \\ \Im(\boldsymbol{\Psi}^{(n)}) & \Re(\boldsymbol{\Psi}^{(n)}) \end{bmatrix}. \tag{24}$$

The CMT-BCS algorithm exploits the group sparsity between the real and imaginary parts of the sparse entries, $\Re(\mathbf{u}^{(n)})$ and $\Im(\mathbf{u}^{(n)})$, and the solution of $\mathbf{u}^{(n)} = \Re(\mathbf{u}^{(n)}) + j\Im(\mathbf{u}^{(n)})$ converges to a K-sparse solution, whose indices correspond to estimates of acceleration of the K ground moving targets, $\hat{\mathbf{a}}^{(k)} = \left[\hat{a}_x^{(k)}, \hat{a}_y^{(k)}, 0\right]^T$, where $k = 1,\cdots,K$. The estimated accelerations are used in the following to estimate the respective target velocities.

3.2.3 Estimation of velocity of multiple targets

For estimating velocity vectors of K targets, we again exploit the group sparsity-based signal recovery method. Define an M-element complex observation vector $\mathbf{y}'^{(n)}$, corresponding to the nth broadcast station, which stacks the M azimuthal samples of the matched filter output, as defined in (9). As such, we define N observation vectors corresponding to each bistatic link. The 2-D space of the unknown velocity can be modeled as an $N_{vx} \times N_{vy}$ search space such that each point in the discretized space represents a hypothetical target velocity vector, where N_{vx} and N_{vy} denote the number of discrete points used to represent the entire target velocity space along the x-axis and y-axis, respectively. As such, for a given estimate of target acceleration $\hat{\mathbf{a}}^{(k)}$, the p'th hypothetical velocity vector is expressed as $\mathbf{v}_{[p']} = [v_{x,n_{vx}}, v_{y,n_{vy}}, 0]^T$, where $v_{x,n_{vx}}$ and $v_{y,n_{vy}}$ are respectively the n_{vx}th discretized value in the N_{vx} x-direction acceleration points and the n_{vy}th discretized value in the N_{vy} y-direction acceleration points, and $p' = (n_{vy}-1)N_{vx} + n_{vx} \in [1, N_{vx}N_{vy}]$. In this case, the bistatic

range at the mth azimuthal sampling instant, after range compensation, can be expressed as,

$$\begin{aligned}\tilde{R}^{(n,k)}_{[p']}(t_m) = &\left\|\mathbf{p}_0^{(k)} + \mathbf{v}_{[p']}t_m + \hat{\mathbf{a}}^{(k)}t_m^2/2 - \mathbf{b}^{(n)}\right\| \\ &+ \left\|\mathbf{p}_0^{(k)} + \mathbf{v}_{[p']}t_m + \hat{\mathbf{a}}^{(k)}t_m^2/2 - \mathbf{r}_0 - \mathbf{v}_r t_m\right\| \\ &- \|\mathbf{q}^{(k)} - \mathbf{b}^{(n)}\| - \left\|\mathbf{q}^{(k)} - \mathbf{r}_0 - \mathbf{v}_r t_m\right\|.\end{aligned} \tag{25}$$

Therefore, given the estimated acceleration $\hat{\mathbf{a}}^{(k)}$, the output of the receiver matched filter corresponding to the kth target, for the p'th hypothetical target velocity, can be modeled as

$$s^{(n,k)}_{[p']}(t_m) = \exp\left(j2\pi f^{(n)}\tilde{R}^{(n,k)}_{[p']}(t_m)/c\right). \tag{26}$$

Denote $\boldsymbol{\psi}'^{(n,k)}_{[p']} \triangleq \left[s^{(n,k)}_{[p']}(t_1), \cdots, s^{(n,k)}_{[p']}(t_M)\right]^T$ as the collection of $s^{(n,k)}_{[p']}(t_m)$ over the M azimuth samples, and let $\boldsymbol{\Psi}'^{(n,k)} = \left[\boldsymbol{\psi}'^{(n,k)}_{[1]}, \cdots, \boldsymbol{\psi}'^{(n,k)}_{[N_{vx}N_{vy}]}\right]$ be the dictionary matrix corresponding to the kth target. As such, the observation signal vector,

$$\mathbf{y}^{(n)} = \left[s^{(n)}(t_1), \cdots, s^{(n)}(t_M)\right]^T, \tag{27}$$

with $s^{(n)}(t_m)$ being given in (9), can be expressed in terms of the dictionary matrix $\boldsymbol{\Psi}'^{(n,k)}$ and the unknown sparse velocity vector $\mathbf{u}'^{(n,k)}$ as

$$\mathbf{y}^{(n)} = \sum_{k=1}^{K}\boldsymbol{\Psi}'^{(n,k)}\mathbf{u}'^{(n,k)} = \boldsymbol{\Psi}'^{(n)}\mathbf{u}'^{(n)}, \tag{28}$$

where $\boldsymbol{\Psi}'^{(n)} = \left[\boldsymbol{\Psi}'^{(n,1)}, \cdots, \boldsymbol{\Psi}'^{(n,K)}\right]$ and $\mathbf{u}'^{(n)} = \left[(\mathbf{u}'^{(n,1)})^T, \cdots, (\mathbf{u}'^{(n,K)})^T\right]^T$. Note that each vector $\mathbf{u}'^{(n,k)}$ is 1-sparse with the non-zero entry index corresponding to the velocity of the kth target, yielding a K-sparse vector of $\mathbf{u}'^{(n)}$.

As discussed in the previous section, the above problem can be cast as a group sparse problem. Again, we decompose the complex observation into its real and imaginary parts before applying the CMT-BCS algorithm to obtain estimates of velocity of the K ground moving targets, $\hat{\mathbf{v}}^{(k)} = \left[\hat{v}_x^{(k)}, \hat{v}_y^{(k)}, 0\right]^T$, with each velocity estimate being associated with the kth acceleration estimate $\hat{\mathbf{a}}^{(k)}$, for $k = 1, \cdots, K$.

In the analysis so far, a perfect knowledge of the initial positions of the ground moving targets is assumed. However, in practice, such perfect localization of the ground moving targets may not be possible, particularly in the weak signal conditions. Note that a very small position error in the order of a fraction of a wavelength can alter the phase accuracy. In the following, therefore, we consider the estimation of motion parameters of multiple ground moving targets considering an imperfect knowledge of the initial positions of the targets.

3.3 Motion parameter estimation considering an imperfect knowledge of the initial positions of the targets

Define $\mathbf{p}_e^{(k)}$ as the error in the estimation of initial position of the kth target. Following (8), and considering the position error, the range difference is expressed as

$$\begin{aligned}\check{R}^{(n,k)}(t_m) = &\left\|\mathbf{p}_0^{(k)} + \mathbf{p}_e^{(k)} + \mathbf{v}^{(k)}t_m + \mathbf{a}^{(k)}t_m^2/2 - \mathbf{b}^{(n)}\right\| \\ &+ \left\|\mathbf{p}_0^{(k)} + \mathbf{p}_e^{(k)} + \mathbf{v}^{(k)}t_m + \mathbf{a}^{(k)}t_m^2/2 - \mathbf{r}_0 - \mathbf{v}_r t_m\right\| \\ &- \left\|\mathbf{q}^{(k)} - \mathbf{b}^{(n)}\right\| - \left\|\mathbf{q}^{(k)} - \mathbf{r}_0 - \mathbf{v}_r t_m\right\|,\end{aligned} \tag{29}$$

and following (9), the corresponding Doppler signature is expressed as

$$\check{s}^{(n)}(t_m) = \sum_{k=1}^{K}\xi^{(n,k)}\exp\left(j2\pi f^{(n)}\check{R}^{(n,k)}(t_m)/c\right). \tag{30}$$

Let $\mathbf{y} = \left[(\mathbf{y}^{(1)})^T, \cdots, (\mathbf{y}^{(N)})^T\right]^T$ denote a long vector of the azimuthal signal samples across all illuminators, where $\mathbf{y}^{(n)}$ is defined in (27). Similarly, define $\check{\mathbf{y}}^{(n)} = \left[\check{s}^{(n)}(t_1), \cdots, \check{s}^{(n)}(t_M)\right]$ and let $\check{\mathbf{y}} = \left[\check{\mathbf{y}}^{(1)T}, \cdots, \check{\mathbf{y}}^{(N)T}\right]^T$ as the signal vector corresponding to the estimated positions of the targets. As such, the cross-correlation between the vectors $\mathbf{s}$ and $\check{\mathbf{s}}$ is calculated as

$$\begin{aligned}\mathbf{y}^H\check{\mathbf{y}} &= \sum_{n=1}^{N}\left(\mathbf{y}^{(n)}\right)^H\check{\mathbf{y}}^{(n)} \\ &= \sum_{n=1}^{N}\sum_{m=1}^{M}\left(s^{(n)}(t_m)\right)^*\check{s}^{(n)}(t_m) \\ &= \sum_{n=1}^{N}\sum_{m=1}^{M}\sum_{k=1}^{K}|\xi^{(n,k)}|^2 \\ &\quad\times\exp\left(j2\pi f^{(n)}\left(R^{(n,k)}(t_m) - \check{R}^{(n,k)}(t_m)\right)/c\right).\end{aligned} \tag{31}$$

When $\mathbf{p}_e^{(k)} = \mathbf{0}$, (31) yields $\sum_{n=1}^{N}\sum_{m=1}^{M}\sum_{k=1}^{K}\left|\xi^{(n,k)}\right|^2$, which is a direct summation of signal energy across all available bistatic pairs. This results in an overall signal enhancement. However, when the position error is non-zero and unknown, the cross-correlation for each bistatic pair yields a complex value with an unknown phase. As a result, their combined contribution may result in a reduced or even nullified overall signal energy

depending upon the phase interactions among the bistatic pairs. This causes a performance degradation of the 4-D ML search. On the other hand, the two-step sequential method based on group sparsity is robust against such phase discrepancies because the performance of the group sparsity-based method does not directly depend on the coherent combination of the multiple Doppler signatures.

4 Performance analysis

In this section, we derive the CRB for the proposed parameter estimation problem for a general target distribution scenario in an MPR system.

The elements of the Fisher information matrix (FIM) of any complex circularly Gaussian process $\mathbf{x}(t_m) \sim \mathcal{N}(\boldsymbol{\mu}(t_m), \mathbf{R})$ are given by [31]

$$[\mathbf{F}]_{i,j} = \mathrm{tr}\left(\mathbf{R}^{-1}\frac{\partial \mathbf{R}}{\partial \vartheta_i}\mathbf{R}^{-1}\frac{\partial \mathbf{R}}{\partial \vartheta_j}\right) + 2\,\Re\left(\sum_{m=0}^{M-1}\frac{\partial \boldsymbol{\mu}^H(t_m)}{\partial \vartheta_i}\mathbf{R}^{-1}\frac{\partial \boldsymbol{\mu}(t_m)}{\partial \vartheta_j}\right), \tag{32}$$

where $\boldsymbol{\vartheta} = [\vartheta_1, \cdots, \vartheta_Q]^T$ represents the $Q \times 1$ vector of unknown variables, and $i, j \in (1, \cdots, Q)$.

In the given problem, the unknown parameter vector is defined as $\boldsymbol{\vartheta} = (\boldsymbol{\xi}, \mathbf{a}, \mathbf{v})$, where $\boldsymbol{\xi} = \left[\boldsymbol{\xi}^{(1)^T}, \cdots, \boldsymbol{\xi}^{(K)^T}\right]^T$, $\mathbf{a} = \left[\mathbf{a}^{(1)^T}, \cdots, \mathbf{a}^{(K)^T}\right]^T$, and $\mathbf{v} = \left[\mathbf{v}^{(1)^T}, \cdots, \mathbf{v}^{(K)^T}\right]^T$, where the respective unknown vectors corresponding to the kth target are defined as $\boldsymbol{\xi}^{(k)} = \left[\xi^{(1,k)}, \cdots, \xi^{(N,k)}\right]^T$, $\mathbf{a}^{(k)} = \left[a_x^{(k)}, a_y^{(k)}\right]^T$, and $\mathbf{v}^{(k)} = \left[v_x^{(k)}, v_y^{(k)}\right]^T$. As such, the structure of the FIM becomes

$$\mathbf{F} = \begin{bmatrix} \mathbf{F}_{\boldsymbol{\xi}\boldsymbol{\xi}} & \mathbf{F}_{\boldsymbol{\xi}\mathbf{a}} & \mathbf{F}_{\boldsymbol{\xi}\mathbf{v}} \\ \mathbf{F}_{\mathbf{a}\boldsymbol{\xi}} & \mathbf{F}_{\mathbf{a}\mathbf{a}} & \mathbf{F}_{\mathbf{a}\mathbf{v}} \\ \mathbf{F}_{\mathbf{v}\boldsymbol{\xi}} & \mathbf{F}_{\mathbf{v}\mathbf{a}} & \mathbf{F}_{\mathbf{v}\mathbf{v}} \end{bmatrix}. \tag{33}$$

Applying (32) to the observation data model (15), we obtain the elements of $\mathbf{F} \in \mathcal{R}^{(N+4)K\times(N+4)K}$ as

$$[\mathbf{F}]_{i,j} = \frac{2}{\sigma^2}\,\Re\left[\sum_{m=0}^{M-1}\frac{\partial \boldsymbol{\gamma}^H(t_m)}{\partial \vartheta_i}\frac{\partial \boldsymbol{\gamma}(t_m)}{\partial \vartheta_j}\right], \tag{34}$$

where $\vartheta_i, \vartheta_j \in \boldsymbol{\vartheta}$. Following (34),

$$\mathbf{F}_{\boldsymbol{\xi}\boldsymbol{\xi}} = \frac{2}{\sigma^2}\,\Re\left[\sum_{m=0}^{M-1}\frac{\partial \boldsymbol{\gamma}^H(t_m)}{\partial \boldsymbol{\xi}}\frac{\partial \boldsymbol{\gamma}(t_m)}{\partial \boldsymbol{\xi}}\right], \tag{35}$$

where $\boldsymbol{\gamma}(t_m) = \sum_{k=1}^{K}\boldsymbol{\Theta}^{(k)}(t_m)\boldsymbol{\xi}^{(k)}$, and therefore,

$$\frac{\partial \boldsymbol{\gamma}(t_m)}{\partial \boldsymbol{\xi}} = \left[\boldsymbol{\Theta}^{(1)}(t_m), \cdots, \boldsymbol{\Theta}^{(K)}(t_m)\right], \tag{36}$$

and

$$\frac{\partial \boldsymbol{\gamma}^H(t_m)}{\partial \boldsymbol{\xi}} = \left[\boldsymbol{\Theta}^{(1)}(t_m), \cdots, \boldsymbol{\Theta}^{(K)}(t_m)\right]^H. \tag{37}$$

Substituting in (35), we obtain

$$\mathbf{F}_{\boldsymbol{\xi}\boldsymbol{\xi}} = \frac{2}{\sigma^2}\,\Re\left[\sum_{m=0}^{M-1}\left[\boldsymbol{\Theta}^{(1)}(t_m), \cdots, \boldsymbol{\Theta}^{(K)}(t_m)\right]^H \times \left[\boldsymbol{\Theta}^{(1)}(t_m), \cdots, \boldsymbol{\Theta}^{(K)}(t_m)\right]\right]. \tag{38}$$

Similarly,

$$\mathbf{F}_{\boldsymbol{\xi}\mathbf{a}} = \frac{2}{\sigma^2}\,\Re\left[\sum_{m=0}^{M-1}\frac{\partial \boldsymbol{\gamma}^H(t_m)}{\partial \boldsymbol{\xi}}\frac{\partial \boldsymbol{\gamma}(t_m)}{\partial \mathbf{a}}\right], \tag{39}$$

where

$$\frac{\partial \boldsymbol{\gamma}(t_m)}{\partial \mathbf{a}} = \left[\frac{\partial \boldsymbol{\Theta}^{(1)}(t_m)\boldsymbol{\xi}^{(1)}}{\partial a_x^{(1)}}, \frac{\partial \boldsymbol{\Theta}^{(1)}(t_m)\boldsymbol{\xi}^{(1)}}{\partial a_y^{(1)}}, \cdots, \frac{\partial \boldsymbol{\Theta}^{(K)}(t_m)\boldsymbol{\xi}^{(K)}}{\partial a_x^{(K)}}, \frac{\partial \boldsymbol{\Theta}^{(K)}(t_m)\boldsymbol{\xi}^{(K)}}{\partial a_y^{(K)}}\right]. \tag{40}$$

Since

$$\boldsymbol{\Theta}^{(k)}(t_m) = \mathrm{diag}\left\{\left[\exp\left(j2\pi f^{(1)}\tilde{R}^{(1,k)}(t_m)/c\right), \cdots, \exp\left(j2\pi f^{(N)}\tilde{R}^{(N,k)}(t_m)/c\right)\right]^T\right\}, \tag{41}$$

the partial derivatives become

$$\begin{aligned}\frac{\partial \boldsymbol{\Theta}^{(k)}(t_m)\boldsymbol{\xi}^{(k)}}{\partial a_x^{(k)}} &= \mathrm{diag}\left\{\left[\left(j2\pi f^{(1)}/c\right)\exp\left(j2\pi f^{(1)}\tilde{R}^{(1,k)}(t_m)/c\right)\frac{\partial \tilde{R}^{(1,k)}(t_m)}{\partial a_x^{(k)}}, \cdots, \left(j2\pi f^{(N)}/c\right)\exp\left(j2\pi f^{(N)}\tilde{R}^{(N,k)}(t_m)/c\right)\frac{\partial \tilde{R}^{(N,k)}(t_m)}{\partial a_x^{(k)}}\right]\right\}\boldsymbol{\xi}^{(k)} \\ &= \boldsymbol{\Theta}^{(k)}(t_m)\boldsymbol{\Lambda}\boldsymbol{\Upsilon}_{a_x}^{(k)}(t_m)\boldsymbol{\xi}^{(k)},\end{aligned} \tag{42}$$

where $\boldsymbol{\Lambda} = \mathrm{diag}\left\{\left[\left(j2\pi f^{(1)}/c\right), \cdots, \left(j2\pi f^{(N)}/c\right)\right]\right\}$ and $\Upsilon_{a_x}^{(k)}(t_m) = \mathrm{diag}\left\{\left[\frac{\partial \tilde{R}^{(1,k)}(t_m)}{\partial a_x^{(k)}}, \cdots, \frac{\partial \tilde{R}^{(N,k)}(t_m)}{\partial a_x^{(k)}}\right]\right\}$. Similarly,

$$\frac{\partial \boldsymbol{\Theta}^{(k)}(t_m)\boldsymbol{\xi}^{(k)}}{\partial a_y^{(k)}} = \boldsymbol{\Theta}^{(k)}(t_m)\boldsymbol{\Lambda}\boldsymbol{\Upsilon}_{a_y}^{(k)}(t_m)\boldsymbol{\xi}^{(k)}, \tag{43}$$

where $\Upsilon_{a_y}^{(k)}(t_m) = \text{diag}\left\{\left[\frac{\partial \tilde{R}^{(1,k)}(t_m)}{\partial a_y^{(k)}}, \cdots, \frac{\partial \tilde{R}^{(N,k)}(t_m)}{\partial a_y^{(k)}}\right]\right\}$. Thus, $\mathbf{F}_{\boldsymbol{\xi}\mathbf{a}}$ can be calculated as

$$\mathbf{F}_{\boldsymbol{\xi}\mathbf{a}} = \frac{2}{\sigma^2}\,\Re\left[\sum_{m=0}^{M-1}\left[\boldsymbol{\Theta}^{(1)}(t_m),\cdots,\boldsymbol{\Theta}^{(K)}(t_m)\right]^H \cdot\left[\boldsymbol{\Theta}^{(1)}(t_m)\boldsymbol{\Lambda}\boldsymbol{\Upsilon}_{a_x}^{(1)}(t_m)\boldsymbol{\xi}^{(1)}, \boldsymbol{\Theta}^{(1)}(t_m)\boldsymbol{\Lambda}\boldsymbol{\Upsilon}_{a_y}^{(1)}(t_m)\boldsymbol{\xi}^{(1)},\cdots, \boldsymbol{\Theta}^{(K)}(t_m)\boldsymbol{\Lambda}\boldsymbol{\Upsilon}_{a_x}^{(K)}(t_m)\boldsymbol{\xi}^{(K)}, \boldsymbol{\Theta}^{(K)}(t_m)\boldsymbol{\Lambda}\boldsymbol{\Upsilon}_{a_y}^{(K)}(t_m)\boldsymbol{\xi}^{(K)}\right]\right]. \tag{44}$$

Similarly,

$$\mathbf{F}_{\boldsymbol{\xi}\mathbf{v}} = \frac{2}{\sigma^2}\,\Re\left[\sum_{m=0}^{M-1}\left[\boldsymbol{\Theta}^{(1)}(t_m),\cdots,\boldsymbol{\Theta}^{(K)}(t_m)\right]^H \cdot\left[\boldsymbol{\Theta}^{(1)}(t_m)\boldsymbol{\Lambda}\boldsymbol{\Upsilon}_{\nu_x}^{(1)}(t_m)\boldsymbol{\xi}^{(1)}, \boldsymbol{\Theta}^{(1)}(t_m)\boldsymbol{\Lambda}\boldsymbol{\Upsilon}_{\nu_y}^{(1)}(t_m)\boldsymbol{\xi}^{(1)},\cdots, \boldsymbol{\Theta}^{(K)}(t_m)\boldsymbol{\Lambda}\boldsymbol{\Upsilon}_{\nu_x}^{(K)}(t_m)\boldsymbol{\xi}^{(K)}, \boldsymbol{\Theta}^{(K)}(t_m)\boldsymbol{\Lambda}\boldsymbol{\Upsilon}_{\nu_y}^{(K)}(t_m)\boldsymbol{\xi}^{(K)}\right]\right], \tag{45}$$

where $\Upsilon_{\nu_x}^{(k)}(t_m) = \text{diag}\left\{\left[\frac{\partial \tilde{R}^{(1,k)}(t_m)}{\partial \nu_x^{(k)}}, \cdots, \frac{\partial \tilde{R}^{(N,k)}(t_m)}{\partial \nu_x^{(k)}}\right]\right\}$ and $\Upsilon_{\nu_y}^{(k)}(t_m) = \text{diag}\left\{\left[\frac{\partial \tilde{R}^{(1,k)}(t_m)}{\partial \nu_y^{(k)}}, \cdots, \frac{\partial \tilde{R}^{(N,k)}(t_m)}{\partial \nu_y^{(k)}}\right]\right\}$. Likewise, we obtain

$$\mathbf{F}_{\mathbf{aa}} = \frac{2}{\sigma^2}\Re\left[\sum_{m=0}^{M-1}\left[\boldsymbol{\Theta}^{(1)}(t_m)\boldsymbol{\Lambda}\boldsymbol{\Upsilon}_{a_x}^{(1)}(t_m)\boldsymbol{\xi}^{(1)}, \boldsymbol{\Theta}^{(1)}(t_m)\boldsymbol{\Lambda}\boldsymbol{\Upsilon}_{a_y}^{(1)}(t_m)\boldsymbol{\xi}^{(1)}, \cdots, \boldsymbol{\Theta}^{(K)}(t_m)\boldsymbol{\Lambda}\boldsymbol{\Upsilon}_{a_x}^{(K)}(t_m)\boldsymbol{\xi}^{(K)}, \boldsymbol{\Theta}^{(K)}(t_m)\boldsymbol{\Lambda}\boldsymbol{\Upsilon}_{a_y}^{(K)}(t_m)\boldsymbol{\xi}^{(K)}\right]^H \cdot\left[\boldsymbol{\Theta}^{(1)}(t_m)\boldsymbol{\Lambda}\boldsymbol{\Upsilon}_{a_x}^{(1)}(t_m)\boldsymbol{\xi}^{(1)}, \boldsymbol{\Theta}^{(1)}(t_m)\boldsymbol{\Lambda}\boldsymbol{\Upsilon}_{a_y}^{(1)}(t_m)\boldsymbol{\xi}^{(1)},\cdots, \boldsymbol{\Theta}^{(K)}(t_m)\boldsymbol{\Lambda}\boldsymbol{\Upsilon}_{a_x}^{(K)}(t_m)\boldsymbol{\xi}^{(K)}, \boldsymbol{\Theta}^{(K)}(t_m)\boldsymbol{\Lambda}\boldsymbol{\Upsilon}_{a_y}^{(K)}(t_m)\boldsymbol{\xi}^{(K)}\right]\right], \tag{46}$$

$$\mathbf{F}_{\mathbf{av}} = \frac{2}{\sigma^2}\Re\left[\sum_{m=0}^{M-1}\left[\boldsymbol{\Theta}^{(1)}(t_m)\boldsymbol{\Lambda}\boldsymbol{\Upsilon}_{a_x}^{(1)}(t_m)\boldsymbol{\xi}^{(1)}, \boldsymbol{\Theta}^{(1)}(t_m)\boldsymbol{\Lambda}\boldsymbol{\Upsilon}_{a_y}^{(1)}(t_m)\boldsymbol{\xi}^{(1)}, \cdots, \boldsymbol{\Theta}^{(K)}(t_m)\boldsymbol{\Lambda}\boldsymbol{\Upsilon}_{a_x}^{(K)}(t_m)\boldsymbol{\xi}^{(K)}, \boldsymbol{\Theta}^{(K)}(t_m)\boldsymbol{\Lambda}\boldsymbol{\Upsilon}_{a_y}^{(K)}(t_m)\boldsymbol{\xi}^{(K)}\right]^H \cdot\left[\boldsymbol{\Theta}^{(1)}(t_m)\boldsymbol{\Lambda}\boldsymbol{\Upsilon}_{\nu_x}^{(1)}(t_m)\boldsymbol{\xi}^{(1)}, \boldsymbol{\Theta}^{(1)}(t_m)\boldsymbol{\Lambda}\boldsymbol{\Upsilon}_{\nu_y}^{(1)}(t_m)\boldsymbol{\xi}^{(1)},\cdots, \boldsymbol{\Theta}^{(K)}(t_m)\boldsymbol{\Lambda}\boldsymbol{\Upsilon}_{\nu_x}^{(K)}(t_m)\boldsymbol{\xi}^{(K)}, \boldsymbol{\Theta}^{(K)}(t_m)\boldsymbol{\Lambda}\boldsymbol{\Upsilon}_{\nu_y}^{(K)}(t_m)\boldsymbol{\xi}^{(K)}\right]\right], \tag{47}$$

and

$$\mathbf{F}_{\mathbf{vv}} = \frac{2}{\sigma^2}\Re\left[\sum_{m=0}^{M-1}\left[\boldsymbol{\Theta}^{(1)}(t_m)\boldsymbol{\Lambda}\boldsymbol{\Upsilon}_{\nu_x}^{(1)}(t_m)\boldsymbol{\xi}^{(1)}, \boldsymbol{\Theta}^{(1)}(t_m)\boldsymbol{\Lambda}\boldsymbol{\Upsilon}_{\nu_y}^{(1)}(t_m)\boldsymbol{\xi}^{(1)}, \cdots, \boldsymbol{\Theta}^{(K)}(t_m)\boldsymbol{\Lambda}\boldsymbol{\Upsilon}_{\nu_x}^{(K)}(t_m)\boldsymbol{\xi}^{(K)}, \boldsymbol{\Theta}^{(K)}(t_m)\boldsymbol{\Lambda}\boldsymbol{\Upsilon}_{\nu_y}^{(K)}(t_m)\boldsymbol{\xi}^{(K)}\right]^H \cdot\left[\boldsymbol{\Theta}^{(1)}(t_m)\boldsymbol{\Lambda}\boldsymbol{\Upsilon}_{\nu_x}^{(1)}(t_m)\boldsymbol{\xi}^{(1)}, \boldsymbol{\Theta}^{(1)}(t_m)\boldsymbol{\Lambda}\boldsymbol{\Upsilon}_{\nu_y}^{(1)}(t_m)\boldsymbol{\xi}^{(1)},\cdots, \boldsymbol{\Theta}^{(K)}(t_m)\boldsymbol{\Lambda}\boldsymbol{\Upsilon}_{\nu_x}^{(K)}(t_m)\boldsymbol{\xi}^{(K)}, \boldsymbol{\Theta}^{(K)}(t_m)\boldsymbol{\Lambda}\boldsymbol{\Upsilon}_{\nu_y}^{(K)}(t_m)\boldsymbol{\xi}^{(K)}\right]\right]. \tag{48}$$

The partial derivatives of the range difference $\tilde{R}^{(n,k)}(t_m)$ with respect to the x- and y-components of acceleration of the kth target are calculated as

$$\frac{\partial \tilde{R}^{(n,k)}(t_m)}{\partial a_x^{(k)}} = \frac{t_m^2}{2}\left(\frac{p_{0x}^{(k)} + v_x^{(k)}t_m + a_x^{(k)}t_m^2/2 - b_x}{\left\|\mathbf{p}_0^{(k)} + \mathbf{v}^{(k)}t_m + \mathbf{a}^{(k)}t_m^2/2 - \mathbf{b}^{(n)}\right\|} + \frac{p_{0x}^{(k)} + v_x^{(k)}t_m + a_x^{(k)}t_m^2/2 - r_{0_x} - v_{r_x}t_m}{\left\|\mathbf{p}_0^{(k)} + \mathbf{v}^{(k)}t_m + \mathbf{a}^{(k)}t_m^2/2 - \mathbf{r}_0 - \mathbf{v}_r t_m\right\|}\right), \tag{49}$$

and

$$\frac{\partial \tilde{R}^{(n,k)}(t_m)}{\partial a_y^{(k)}} = \frac{t_m^2}{2}\left(\frac{p_{0y}^{(k)} + v_y^{(k)}t_m + a_y^{(k)}t_m^2/2 - b_y}{\left\|\mathbf{p}_0^{(k)} + \mathbf{v}^{(k)}t_m + \mathbf{a}^{(k)}t_m^2/2 - \mathbf{b}^{(n)}\right\|} + \frac{p_{0y}^{(k)} + v_y^{(k)}t_m + a_y^{(k)}t_m^2/2 - r_{0_y} - v_{r_y}t_m}{\left\|\mathbf{p}_0^{(k)} + \mathbf{v}^{(k)}t_m + \mathbf{a}^{(k)}t_m^2/2 - \mathbf{r}_0 - \mathbf{v}_r t_m\right\|}\right). \tag{50}$$

Likewise, the partial derivatives of $\tilde{R}^{(n,k)}(t_m)$ with respect to the x- and y-components of velocity of the kth target are calculated as

$$\frac{\partial \tilde{R}^{(n,k)}(t_m)}{\partial v_x^{(k)}} = t_m\left(\frac{p_{0x}^{(k)} + v_x^{(k)}t_m + a_x^{(k)}t_m^2/2 - b_x}{\left\|\mathbf{p}_0^{(k)} + \mathbf{v}^{(k)}t_m + \mathbf{a}^{(k)}t_m^2/2 - \mathbf{b}^{(n)}\right\|} + \frac{p_{0x}^{(k)} + v_x^{(k)}t_m + a_x^{(k)}t_m^2/2 - r_{0_x} - v_{r_x}t_m}{\left\|\mathbf{p}_0^{(k)} + \mathbf{v}^{(k)}t_m + \mathbf{a}^{(k)}t_m^2/2 - \mathbf{r}_0 - \mathbf{v}_r t_m\right\|}\right), \tag{51}$$

and

$$\frac{\partial \tilde{R}^{(n,k)}(t_m)}{\partial v_y^{(k)}} = t_m\left(\frac{p_{0y}^{(k)} + v_y^{(k)}t_m + a_y^{(k)}t_m^2/2 - b_y}{\left\|\mathbf{p}_0^{(k)} + \mathbf{v}^{(k)}t_m + \mathbf{a}^{(k)}t_m^2/2 - \mathbf{b}^{(n)}\right\|} + \frac{p_{0y}^{(k)} + v_y^{(k)}t_m + a_y^{(k)}t_m^2/2 - r_{0_y} - v_{r_y}t_m}{\left\|\mathbf{p}_0^{(k)} + \mathbf{v}^{(k)}t_m + \mathbf{a}^{(k)}t_m^2/2 - \mathbf{r}_0 - \mathbf{v}_r t_m\right\|}\right). \tag{52}$$

By definition, the CRB on estimation performance of the unknown variables is determined by the respective diagonal elements of the inverse of the FIM.

5 Simulation results

In the simulations, we consider a geolocation scenario as illustrated in Figure 1, where seven digital audio broadcast (DAB) stations [32] are respectively located at $[10, -10, 0.1]^T$ km, $[-10, 12, 0.1]^T$ km, $[10, -18, 0.1]^T$ km, $[0, -20, 0.1]^T$ km, $[-10, -10, 0.1]^T$ km, $[-5, 15, 0.1]^T$ km, and $[-5, 5, 0.1]^T$ km. The respective carrier frequencies of these seven illuminators are 225, 227, 229, 231, 233, 235, and 237 MHz.

The initial position of the airborne receiver is $[0, 0, 5]^T$ km, and it moves with a constant velocity of $[150, 0, 0]^T$ m/s. The simulation results illustrate the performance of the proposed method over a 20-dB range of the input SNR, which is defined per sample in the fast time. It is important to note that, since the receiver data is sampled at 2.048 MHz and the matched filter output yields a 200-Hz azimuthal sampling frequency, a processing gain of 40.1 dB is achieved at the output of the matched filter. The overall CPI is assumed to be 2 s, which generates 400 azimuthal samples per illuminator. The amplitude parameter $\xi^{(n,k)}$ in (9) is assumed to be unity for all n and k.

We consider two ground moving targets which are closely located, respectively, at $[0, 14, 0]^T$ km and $[0.05, 14, 0]^T$ km. The first target is assumed to be moving with an initial speed of $[-7, -7, 0]^T$ m/s and an acceleration of $[-3, -3, 0]^T$ m/s^2, whereas the second target is assumed to be moving with an initial speed of $[7, 7, 0]^T$ m/s and an acceleration of $[3, 3, 0]^T$ m/s^2.

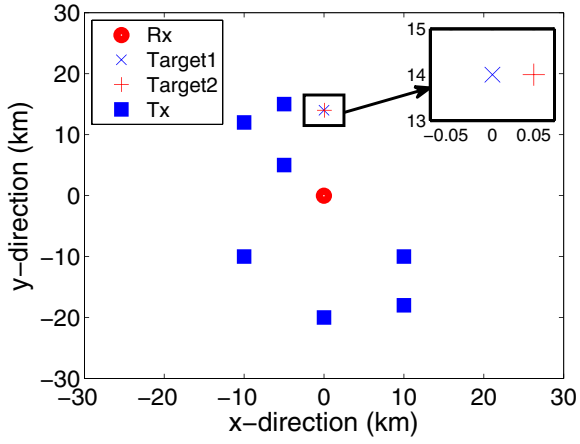

Figure 1 Geometry of the multi-static, multi-target passive system. The relative positions of transmitters, receiver, and two closely spaced ground moving targets are illustrated.

The spectrogram and the ambiguity function of Doppler signatures of two targets corresponding to the first illuminator are presented in Figure 2 at two different SNR conditions. For high SNR applications, as illustrated in Figure 2a,b, the spectrogram constitutes two distinct lines corresponding to the respective initial frequency and chirp rate of the Doppler signatures of the two targets. The ambiguity function, on the other hand, constitutes two distinct straight lines passing through the origin, with different slopes depending on the respective chirp rates. As such, the chirp parameters can be reliably estimated for each bistatic link using time-frequency analysis-based methods, and subsequently, the respective motion parameters can be estimated using (11) by using the standard least squares (LS) methods. However, when the input SNR is low, as evident in Figure 2c,d, it is difficult to reliably obtain chirp parameters corresponding to each bistatic link. The chirp parameter estimation process in the presence of additive white Gaussian noise suffers a rapid performance degradation below a certain SNR threshold. This necessitates a mechanism to combine signal energy from all available bistatic links which, however, is difficult to implement directly in the time-frequency domain. By exploiting sparsity-based signal reconstruction, the ML and the two-step sequential methods, respectively, provide a means to coherently and non-coherently combine Doppler signatures from all available links. They result in an overall signal enhancement, and consequently, the threshold is reached at a lower SNR as compared to the traditional time-frequency analysis-based methods.

The performance of the sparse signal reconstruction-based methods is compared against the CRB formulated in (34) for the underlying problem. For the given simulation scenario, we obtain the root-mean-square error (RMSE) of the estimated acceleration and velocity through 100 independent trials, and the results are, respectively, presented in Figure 3a,b.

Results for one of the targets are depicted in Figure 3a,b, and similar qualitative results are obtained for the parameters of the second target as well. The error performance of the sequential estimator is also compared against those obtained from a 4-D ML estimation and traditional time-frequency analysis-based technique (e.g., using chirp-Fourier transform). The results shown in Figure 3a,b illustrate that the RMSE of ML estimates of the motion parameters are approximately 3 dB higher than the respective CRB. Similar results are presented in [33,34]. Simulation results show that the sequential method outperforms the parameter estimation technique based on the chirp-Fourier transform since the threshold effect for this method is delayed when compared to the chirp transform-based method. Also, as illustrated in Figure 4, the availability of more transmitters can be exploited to further lower the SNR threshold using the

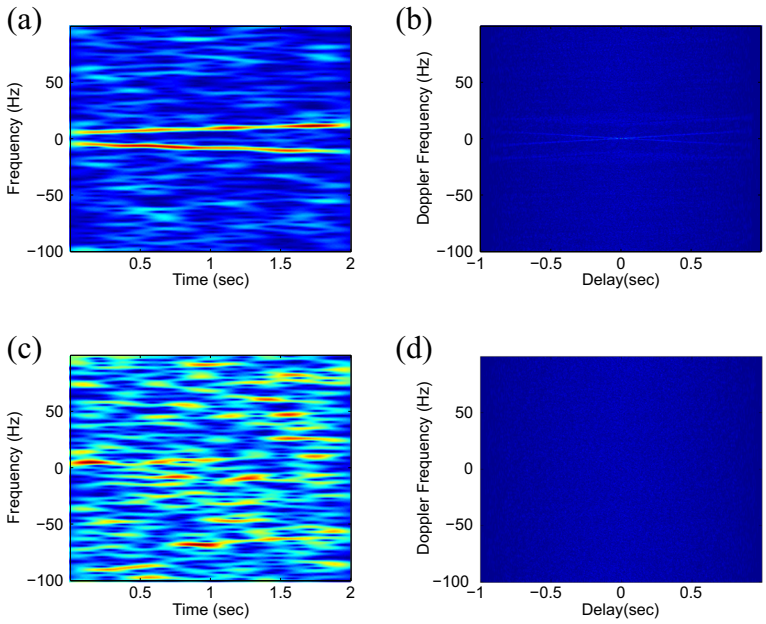

Figure 2 Spectrogram and ambiguity function of Doppler signature for two targets at high and low SNR. (a) Spectrogram (SNR= −45 dB). **(b)** Ambiguity function (SNR= −45 dB). **(c)** Spectrogram (SNR= −53 dB). **(d)** Ambiguity function (SNR= −53 dB).

proposed method. As discussed in Section 3, representation of target motion parameters in a discretized parameter space may yield an off-grid problem. However, in the simulated example, we have defined the grid resolution fine enough to match the CRB, such that the performance is robust even if the true parameter is off-grid. Specifically, grid resolutions used in this simulated example are 0.05 m/s^2 for acceleration and 0.01 m/s for velocity estimation, respectively.

As discussed in Section 4, errors in the assumed or estimated initial positions of the targets result in phase differences among the Doppler signatures corresponding to different bistatic links. In such a situation, depending upon the phase interactions, the individual Doppler signatures may destructively add to each other, yielding a significant reduction in overall signal energy accumulation through a coherent fusion process. As such, the ML search-based motion parameter estimation suffers a performance degradation in case of an imperfect knowledge about the initial positions of the targets. On the other hand, the sequential method does not rely on coherent combining of the Doppler signatures for overall signal enhancement and, hence, is robust against such phase misalignment. In order to illustrate such situation, we consider a position error of $[1, 0, 0]^T$ m, which is approximately equal to the wavelength of operation, in the estimation of the initial positions of both targets. It is evident in Figure 5 that the ML search-based motion parameter error suffers a significant performance loss, whereas the two-step sequential method is robust against such localization error, which is an observation of high practical significance.

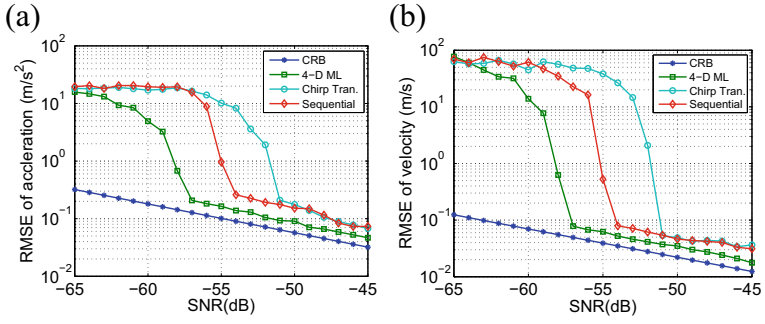

Figure 3 Error performance of motion parameter estimation. (a) Acceleration. **(b)** Velocity.

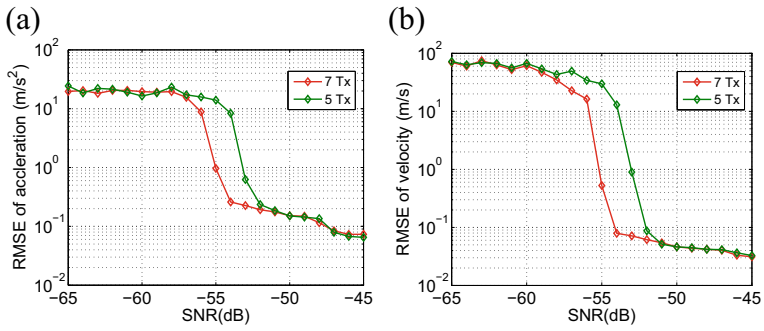

Figure 4 Comparison of RMSE of parameter estimation using different numbers of transmitters. (a) Acceleration. **(b)** Velocity.

It is important to note that there are two sources of error that are inherently associated with the target acceleration estimation using the proposed method. Since the ambiguity function, defined in (18), is bilinear, the effect of noise is enhanced, resulting in a performance degradation as compared to its linear transform counterpart. Furthermore, since matrix mapping the chirp parameters to the respective motion parameters, defined in (12), is not exactly block diagonal, the target velocity does have a small effect on the chirp rate. This introduces an estimation error in the acceleration because target velocity is not considered in (19). The significance of the error is proportional to the ratio of velocity of the receiver platform to the target-receiver separation. That is, the effect of this off-diagonal block becomes insignificant for distant targets. In the simulated example, the off-diagonal term is small, yielding negligible acceleration estimation error. Specifically, in the simulated example, the off-diagonal term is approximately $[0.015, 0, 0]^T$ 1/s and the corresponding acceleration estimation error is approximately 0.004 m/s^2. Velocity estimation, on the other hand, involves a linear process. Therefore, it does not suffer from performance degradation due to bilinear effects as in acceleration estimation. However, the error which occurred in the estimated target acceleration propagates to the velocity estimation, and the significance of such error propagation depends on the duration of the CPI. Also, when the target motion parameters are closely located in the parameter space, the performance deteriorates specially in low SNR conditions.

6 Conclusions

We have developed novel methods for the estimation of motion parameters of multiple closely located ground moving targets in a multi-static passive radar platform. By exploiting the fact that the Doppler signatures of the targets corresponding to different bistatic links share the same target motion parameters as a common sparse support in the discretized parameter search space, the underlying problem is reformulated as a group sparse signal reconstruction problem. The sparse signal reconstruction-based methods allow for the fusion of data from all bistatic links, which is not possible in traditional time-frequency analysis-based methods. The two-step sequential method emphasizes on decoupling the effects of target acceleration and velocity on the Doppler signature and obtains a sequential estimation of the target motion parameters to avoid the need for a computationally demanding multi-dimensional exhaustive search. It is shown that the sequential method also outperforms

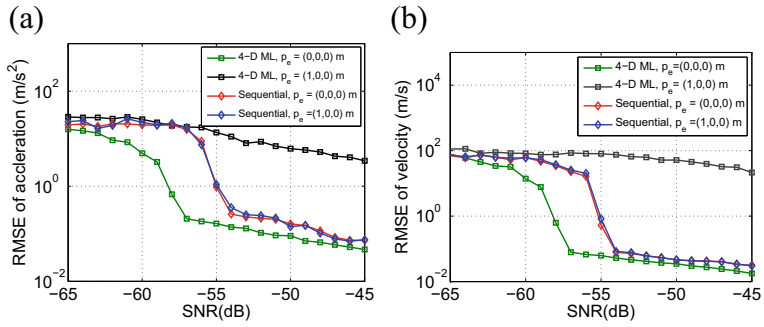

Figure 5 Comparison of RMSE of parameter estimation considering an imperfect knowledge of initial target positions. (a) Acceleration. **(b)** Velocity.

the maximum likelihood search-based parameter estimation in cases where the initial positions of the targets is not precisely known. The performance of the proposed estimators is validated by simulations, and it is shown that these approaches outperform the time-frequency analysis-based methods and closely approaches the Cramér-Rao Bound.

Competing interests
The authors declare that they have no competing interests.

Acknowledgements
The work of S. Subedi, Y. D. Zhang, and M. G. Amin was supported in part by a subcontract with Defense Engineering Corporation for research sponsored by the Air Force Research Laboratory under Contract FA8650-12-D-1376 and by a subcontract with Dynetics, Inc. for research sponsored by the Air Force Research Laboratory under Contract FA8650-08-D-1303. Part of the work was presented in the 2014 IEEE International Conference on Acoustics, Speech, and Signal Processing [35].

Author details
[1]Center for Advanced Communications, Villanova University, Villanova, PA 19085, USA. [2]RF Technology Branch, Air Force Research Laboratory, AFRL/RYMD, Dayton, OH 45433, USA.

Received: 28 June 2014 Accepted: 9 October 2014
Published: 24 October 2014

References

1. H Griffitths, N Long, Television-based bistatic radar. IEE Proc. Commun. Radar Signal Proc. **133**(7), 649–657 (1986)
2. S Subedi, YD Zhang, MG Amin, B Himed, in *Proceedings of European Signal Processing Conference*. Robust motion parameter estimation in multistatic passive radar (Marrakech, Morocco, Sept. 2013)
3. GR Curry, *Radar System Performance Modeling, 2nd ed*, (Artech House, Norwood, 2005)
4. MI Skolnik, *Introduction to Radar Systems, 3rd ed*, (McGraw-Hill, New York, 2001)
5. A Hassanien, SA Vorobyov, AB Gershman, Moving target parameter estimation in noncoherent MIMO radar systems. IEEE Trans. Signal Process. **60**(5), 2354–2361 (2012)
6. Q He, RS Blum, H Godrich, AM Haimovich, in *Proceedings of Annual Conference on Information Sciences and Systems*. Cramer-Rao bound for target velocity estimation in MIMO radar with widely separated antennas (Princeton, NJ, Mar. 2008)
7. Q He, RS Blum, AM Haimovich, Noncoherent MIMO radar for location and velocity estimation: more antennas means better performance. IEEE Trans. Signal Process. **58**(7), 3661–3680 (2010)
8. Y Zhang, MG Amin, F Ahmad, in *Proceedings of Asilomar Conference on Signals, Systems, and Computers*. A novel approach for moving multi-target localization using dual frequency radars and time-frequency distributions (Pacific Grove, CA, Nov. 2007), pp. 1817–1821
9. F Zhou, R Wu, M Xing, Z Bao, Approach for single channel SAR ground moving target imaging and motion parameter estimation. IET Radar, Sonar Navigation. **1**(1), 59–66 (2007)
10. SQ Zhu, GS Liao, Y Qu, ZG Zhou, in *Proceedings of IEEE Radar Conference*. Ground moving targets detection and unambiguous motion parameter estimation based on multi-channel SAR system, (April 2009), pp. 1–4
11. M Kubica, V Kubica, X Neyt, J Raout, S Roques, M Acheroy, in *Proceedings of IEEE Radar Conference*. Optimum target detection using illuminators of opportunity, (April 2006), pp. 24–27
12. AP Whitewood, BR Muller, HD Griffiths, CJ Baker, in *Proceedings of IEEE Radar Conference*. Bistatic synthetic aperture radar with application to moving target detection, (Sept. 2003), pp. 529–534
13. A Scaglione, S Barbarossa, in *Proceedings of IEEE Radar Conference*. Estimating motion parameters using parametric modeling based on time-frequency representations (Syracuse, NY, Oct. 1997)
14. S Stankovi, I Djurovi, Motion parameter estimation by using time-frequency representations. IEEE Electron. Lett. **37**(24), 1446–1448 (2001)
15. YD Zhang, B Himed, in *Proceedings of IEEE Radar Conference*. Moving target parameter estimation and SFN ghost rejection in multistatic passive radar (Ottawa, Canada, April 2013)
16. S Peleg, B Porat, The Cramer-Rao lower bound for signals with constant amplitude and polynomial phase. IEEE Trans. Signal Process. **39**(3), 749–752 (1991)
17. S Saha, SM Kay, Maximum likelihood parameter estimation of superimposed chirps using Monte Carlo importance sampling. IEEE Trans. Signal Process. **50**(2), 224–230 (2002)
18. C Berger, B Demissie, J Heckenbach, P Willett, S Zhou, Signal processing for passive radar using OFDM waveforms. IEEE J. Selected Topics Signal Process. **4**(1), 226–238 (2010)
19. RP Perry, RC DiPietro, R Fante, in *Proceedings IEEE Radar Conference*. Coherent integration with range migration using Keystone formatting (Boston, MA, April 2007), pp. 863–868
20. B Boashash, *Time Frequency Signal Analysis and Processing: A Comprehensive Reference*. (Elsevier, Oxford, UK, 2003)
21. GC Gaunaurd, HC Strifors, Signal analysis by means of time-frequency (Wigner-type) distributions-applications to sonar and radar echoes. Proc. IEEE. **84**(9), 1231–1248 (1996)
22. V Chen, H Ling, Joint time-frequency analysis for radar signal and image processing. IEEE Signal Process. Mag. **16**(2), 81–93 (1999)
23. HB Sun, G-S Liu, H Gu, W-M Su, Application of the fractional Fourier transform to moving target detection in airborne SAR. IEEE Trans. Aero. Electron. Syst. **38**(4), 1416–1424 (2002)
24. S Barbarossa, Analysis of multicomponent LFM signals by a combined Wigner-Hough transform. IEEE Trans. Signal Process. **43**(6), 1511–1515 (1995)
25. EVD Berg, M Friedlander, Probing the Pareto frontier for basis pursuit solutions. SIAM J. Sci. Comput. **31**(2), 890–912 (2008)
26. M Yuan, Y Lin, Model selection and estimation in regression with grouped variables. J. Roy. Stat. Soc. B. **68**(1), 49–67 (2006)
27. L Zelnik-Manor, K Rosenblum, YC Eldar, Sensing matrix optimization for block-sparse decoding. IEEE Trans. Signal Process. **59**(9), 4300–4312 (2011)
28. S Ji, D Dunson, L Carin, Multitask compressive sensing. IEEE Trans. Signal Process. **57**(1), 92–106 (2009)
29. Q Wu, YD Zhang, MG Amin, B Himed, in *Proceedings of IEEE International Conference on Acoustics, Speech, and Signal Processing (ICASSP)*. Complex multi-task Bayesian compressive sensing (Florence, Italy, May 2014)
30. M Carlin, P Rocca, G Oliveri, F Viani, A Massa, Directions-of-arrival estimation through Bayesian compressive sensing strategies. IEEE Trans. Antenn. Propag. **61**(7), 3828–3838 (2013)
31. S Kay, *Fundamentals of Statistical Signal Processing: Estimation Theory*. (Prentice-Hall, Englewood Cliffs, 1993)
32. C Coleman, H Yardley, in *Proceedings of International Conference on Radar*. DAB based passive radar: performance calculations and trials (Adelaide, Australia, Sept. 2008), pp. 691–694
33. B Friedlander, JM Francos, Estimation of amplitude and phase parameters of multicomponent signals. IEEE Trans. Signal Process. **43**(4), 917–925 (1995)
34. S Peleg, B Friedlander, in *Proceedings of IEEE-SP International Symposium of the Time-Frequency and Time-Scale Analysis*. A technique for estimating the parameters of multiple polynomial phase signals (Victoria, Canada, Oct. 1992)
35. S Subedi, YD Zhang, MG Amin, B Himed, in *Proceedings of IEEE International Conference on Acoustics, Speech, and Signal Processing (ICASSP)*. Motion parameter estimation of multiple targets in multistatic radar through sparse signal recovery (Florence, Italy, May 2014)

doi:10.1186/1687-6180-2014-157
Cite this article as: Subedi *et al.*: **Motion parameter estimation of multiple ground moving targets in multi-static passive radar systems.** *EURASIP Journal on Advances in Signal Processing* 2014 **2014**:157.